Struct Multidisc Optim
DOI 10.1007/s00158-014-1127-6

RESEARCH PAPER

A numerical form-finding method for the minimal surface of membrane structures

M. Shimoda · K. Yamane

Received: 1 August 2013 / Revised: 16 April 2014 / Accepted: 23 May 2014

Abstract This paper proposes a convenient numerical form-finding method for designing the minimal surface, or the equally tensioned surface of membrane structures with specified arbitrary boundaries. Area minimization problems are formulated as a distributed-parameter shape optimization problem. The internal volume or the perimeter is added as a constraint according to the structure type such as a pneumatic or a suspension membrane. It is assumed that the membrane is varied in the out-of-plane and/or the in-plane direction to the surface. The shape sensitivity function for each problem is derived using the material derivative method. The minimal surface is determined without shape parameterization by the free-form optimization method, a gradient method in the Hilbert space, where the shape is varied by the traction force in proportion to the sensitivity function under the Robin boundary condition. The calculated results show the effectiveness and practical utility of the proposed method for optimal form-finding of membrane structures.

Keywords Membrane structure · Formfinding · Shape optimization · Minimal surface · Free form

1 Introduction

Sheet-like solids such as cloth and resin film are called membranes, which are very thin and flexible. Mechanical characteristics of a membrane structure include negligible bending, while maintaining its shape and carrying external force with stresses consisting of in-plane tensile stress and shear stress. Both isotropic and anisotropic materials are used for membranes. Membrane structures have many advantages: they contribute to safety and economy, they are lightweight and not bulky, and they have good aesthetic aspects due to their curved surface and translucency. By taking advantage of these characteristics, various membrane structures have been developed and widely used for industrial products. In the field of architecture, membranes tend to be used as roofs because they are suitable for constructing longspan structures, allow a short construction period, and provide excellent earthquake resistance. They can also be used for functional structures such as automotive airbags that absorb impact energy and as the sails of yachts and the wings of paragliders for generating lift. Further, they are used for airships, balloons playground equipment, and daily commodities such as umbrellas and chairs.

As mentioned above, membranes must maintain their shapes only by means of in-plane tension due to their negligible bending stiffness, which makes it difficult for them to maintain the required shapes. Therefore form-finding is vitally important in the design process. In order to keep the desired shape and to secure sufficient stiffness and strength against self-weight and external force, initial tensions must be appropriately applied to membranes. Membrane structures are classified into the pneumatic (air-support) membrane type in which tensions are generated by differential pressure and the non-pneumatic membrane type to which tensions are applied by mechanical force (Otto 1973). Non-pneumatic structures are also classified into the frame membrane type and the suspension membrane type. Non-pneumatic structures must have non-positive Gaussian curvature over the whole surface to maintain the shape.

M. Shimoda (✉)
Toyota Technological Institute, 2-12-1 Hisakata,
Tenpaku-ku, Nagoya, 468-8511 Japan
e-mail: shimoda@toyota-ti.ac.jp

K. Yamane
Graduate School of Toyota Technological Institute, Nagoya, Japan

Published online: 09 August 2014

Fig. 1 shows the classification of membrane structures. Regardless of the structure type, membranes cannot be expected to have much bearing capacity due to their thinness even if they are made of strong materials. Therefore designers need to determine the membrane shape so that there is a uniform stress field across the entire surface.

It is well known that a shape with a uniform stress field conforms to the minimal surface which has zero mean curvature across the surface if the deformation due to the self-weight is negligible. If a constraint condition is given, it has a certain amount of curvature. Such a surface with a constant curvature is also regarded as the minimal surface under the constraint condition. Even though these surfaces are just ideal ones and different from the optimal shape subjected to an external force, they are considered as the basis of an optimal shape. Therefore finding this basic shape is imperative and many approaches using experiments and calculations have been tried. A physical experiment using a soap film has been applied for centuries as this approach can easily find minimal surfaces with frames (Otto 1973). It was also mathematically studied as a variational problem and many minimal surface functions were found (Gray 1998). However it is difficult to find minimal surfaces taking account of structural characteristics or aesthetic satisfaction. Thus the applicable range of both approaches can never be extended. In order to solve that disadvantage, versatile numerical solutions using computer have been studied. Monterde (2004) determined approximate minimal surfaces using Bezier surfaces and Arnal et al. () also used them to obtain surfaces with a constant mean curvature. These are efficient methods since the number of design variables is reduced by shape parameterization, while the obtained shape and its characteristics are restricted by the parameter. Bletzinger et al. (2010) presented a method that simulates classical physical experiments such as the soap film and the hanging model by finite element analysis taking geometric non-linearity into consideration. Though the computation cost is considerable, it does not require shape parameterization and is applicable both to cases involving an anisotropic material and ones where an initial tension is applied. They also proposed a method combined with mesh regularization (Bletzinger 2005). Linkwitz (1999) proposed Force density method mainly aiming at form-finding for cable-net structures, and that method was successfully extended to triangular element, allowing membrane analyses. Pan and Xu (2011) showed minimal subdivision surfaces with given boundaries using the mean curvature flow, a secondorder geometric partial differential equation. Their method finds a minimal surface while subdividing the meshes for mesh refinement.

In the wake of these studies, in this paper we propose a new numerical solution for finding a minimal surface, i.e. an equally tensioned surface of membrane structures with an arbitrarily specified boundary. The authors have been developing a non-parametric free-form optimization method without shape parameterization for the optimal shape of three-dimension continua (Shimoda et al. 1998), shell structures (Shimoda and Tsuji 2006; Shimoda and Liu 2014) and frame structures (Shimoda et al. 2014). This study presents a non-parametric, or a node-based solution for form-finding of membrane structures by applying our free-form optimization method for shell structures. This method finds a minimal surface by formulating the form-finding problem as a distributed-parameter shape optimization problem based on the classical variational method, and applying the sensitivity function derived by the material derivative formula to the modern numerical free-form optimization method. The advantages of this method include efficiency for treating large-scale problems and the ability to obtain a smooth shape. In the shape design of a membrane structure, the shape could vary in the in-plane direction and/or out-of-plane direction. We consider both directions as design variables. Form-finding with constraint conditions (e.g. perimeter and internal volume) can be performed for a pneumatic membrane structure, a frame membrane structure and a suspension membrane structure.

In the following sections, we will first show the formulations of minimal surface problems as distributed-parameter optimization problems and derive each sensitivity function which is called the shape gradient function. Then the free-form optimization method for membrane structures will be proposed. Finally we will show examples of each type of membrane structure.

2 Domain variation of membrane structure

2.1 Definition of shape variation for free-form design

As shown in Fig. 2 consider that a membrane having an initial domain A with the boundary ∂A is varied into one

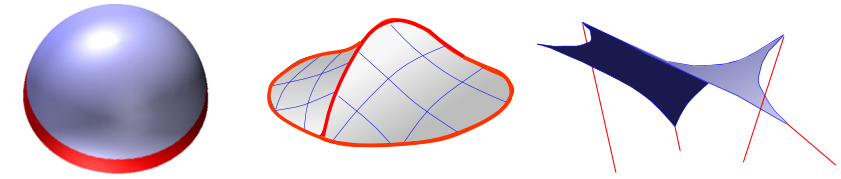

(a) Pneumatic membrane (b) Frame membrane (c) Suspension membrane

Fig. 1 Classification of membrane structures

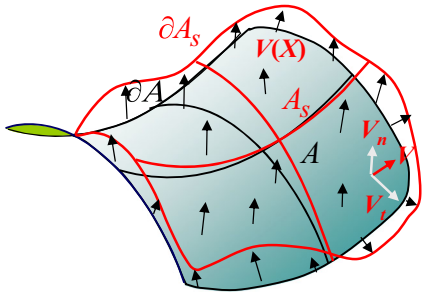

Fig. 2 Shape variation of membrane by $\boldsymbol{V}$

having domain A_s with the boundary ∂A_s by the shape variation (the design velocity field) $\boldsymbol{V}$ distributed across the surface It is assumed that the boundary ∂A is included in the domain A ($\partial A \subset A$) and that the thickness h is constant during the deformation. The shape variation. $\boldsymbol{V}$ consists of the out-of-plane variation $\boldsymbol{V}_n(\equiv (\boldsymbol{V}\cdot\boldsymbol{n})\boldsymbol{n})$ which deforms in the normal direction to the surface and the in-plane variation $\boldsymbol{V}_t(\equiv (\boldsymbol{V}\cdot\boldsymbol{t})\boldsymbol{t})$ which deforms in the tangential direction to the surface. The notations $\boldsymbol{n}$ and $\boldsymbol{t}$ indicate the outward unit normal and tangential vectors to the surface, respectively. The membrane shape is varied by $\boldsymbol{V}_n(\boldsymbol{X}_s)$ distributed on A and $\boldsymbol{V}_t(\boldsymbol{X}_s)$ distributed on ∂A since $\boldsymbol{V}_t(\boldsymbol{X}_s)$ does not affect the shape variation except on ∂A. The shape variation is expressed by the piecewise smooth mapping $T_S\boldsymbol{X} \in A \mapsto \boldsymbol{X}_s(\boldsymbol{X}) \in A_s$, $0 \le s \le \varepsilon$ (Choi and Kim 2005; Azegami 1994), where ε and $(\cdot)_s$ indicate a small integer and the iteration history of the shape variation equivalent to time. Using the relations $\boldsymbol{X}_s = T_s(\boldsymbol{X})$, $A_s = T_s(A)$, the small shape variation around the s-th variation is expressed as

$$T_{s+\Delta s}(\boldsymbol{X}) = T_s(\boldsymbol{X}) + \Delta s\boldsymbol{V} + O(|\Delta s|^2), \tag{1}$$

where the design velocity field $\boldsymbol{V}(\boldsymbol{X}_s) = \partial T_s(\boldsymbol{X})/\partial s$ is given as the Euler derivative of the mapping $T_s(\boldsymbol{X})$, and $O(|\Delta s|^2)$ is assumed to be neglected as a high-order term. The optimal design velocity field $\boldsymbol{V}(\boldsymbol{X_s})$ is determined by the free-form optimization method proposed in this paper which will be explained later. The design velocity field $\boldsymbol{V}(\boldsymbol{X}_s)$ is approximated to $\boldsymbol{V}(\boldsymbol{X})$ under the assumption of infinitesimal shape variation.

2.2 Formulae of the material derivative

The shape gradient function, i.e. the variation of evaluation functional with respect to shape variation, is determined by the material derivative method (Choi and Kim 2005). In this section we will present the following formulae for the membrane structure. When the evaluation functional J is given as a surface integration of the distribution function ϕ_s, which is written as

$$J = \int_{A_s} \phi_s dA \tag{2}$$

the material derivative $\dot{J}$ is expressed as

$$\dot{J} = \int_A \varphi' dA + \int_A (\varphi_{,i}n_i + \varphi H_A)V_n dA + \int_{\partial A} \varphi V_t d\Gamma \tag{3}$$

where H_A indicates twice the mean curvature distributed on the surface. The notations $V_n = n_i V_i$ and $V_t = t_i V_i$ are the normal and tangential components of $\boldsymbol{V}$, respectively. The notation $(\cdot)'$ indicates a shape derivative (Choi and Kim 2005) and has a relation of $\dot{(\cdot)} = (\cdot)' + (\cdot)_{,i}V_i$. In this paper, the tensor subscript notation uses Einstein's summation convention and a partial differential notation for the spatial coordinates $(\cdot)_{,i} = \partial(\cdot)/\partial x_i$. When the evaluation functional J is given as a volume integration of the distribution function ϕ_s, which is written as

$$J = \int_{\Omega_s} \phi_s d\Omega, \tag{4}$$

the material derivative $\dot{J}$ is expressed as

$$\dot{J} = \int_\Omega \varphi' d\Omega + \int_A \varphi V_n dA. \tag{5}$$

When the evaluation functional J is given as a boundary (i.e., edge) integration of the distribution function ϕ_s, which is written as

$$J = \int_{\partial A_s} \phi_s d\Gamma, \tag{6}$$

the material derivative $\dot{J}$ is expressed as

$$\dot{J} = \int_{\partial A} \{\varphi' + (\varphi_{,i}t_i + \varphi H_{\partial A})V_t\} d\Gamma, \tag{7}$$

where $H_{\partial A}$ expresses the curvature distributed on the boundary ∂A

3 Form-finding problems of membrane structures and derivation of shape gradient function

In order to find the minimal surface, the area of a membrane is defined as an objective functional. In addition to the boundary shape, the internal volume or perimeter is set as another constraint condition according to the structure type. The constraint value of perimeter length or internal volume is applied to a tentative initial shape in order to determine the final shape of a membrane. In this section, we will formulate a distributed-parameter shape optimization problem for each type of membrane structure, so as to determine the design velocity field that leads to the minimal surface, and then the shape gradient function will be derived.

3.1 Frame membrane structure problem

Consider a shape optimization problem for minimizing the area of a frame membrane structure like that shown

in Fig. 1b. When an initial membrane shape A_0 and a specified boundary shape formed by the frame which may be an open boundary are given, this problem is expressed as

$$\text{Given} \quad A_0, \tag{8}$$

$$\text{find} \quad \boldsymbol{V}\ (\text{or}\ A_s), \tag{9}$$

$$\text{that minimizes} \quad A\left(=\int_A dA\right). \tag{10}$$

The Lagrange functional L for this problem is expressed as

$$L(A)=\int_A dA. \tag{11}$$

The material derivative $\dot{L}$ of the Lagrange functional L with respect to shape variation is expressed as

$$\dot{L}=<G_A\boldsymbol{n},\boldsymbol{V}>_A+<G_{\partial A}\boldsymbol{t},\boldsymbol{V}>_{\partial A},\quad \boldsymbol{V}\in C_\Theta, \tag{12}$$

where the notations of $<G_A\boldsymbol{n},\boldsymbol{V}>_A$ and $<G_{\partial A}\boldsymbol{t},\boldsymbol{V}>_{\partial A}$ are defined as

$$<G_A\boldsymbol{n},\boldsymbol{V}>_A\equiv\int_A G_A\boldsymbol{n}\cdot\boldsymbol{V}dA=\int_A G_A V_n dA, \tag{13}$$

$$<G_{\partial A}\boldsymbol{t},\boldsymbol{V}>_{\partial A}\equiv\int_{\partial A} G_{\partial A}\boldsymbol{t}\cdot\boldsymbol{V}d\Gamma=\int_{\partial A} G_{\partial A}V_t d\Gamma, \tag{14}$$

$$G_A=H_A, \tag{15}$$

$$G_{\partial A}=H_{\partial A}, \tag{16}$$

where C_Θ indicates the admissible function space that satisfies the specified geometric boundary condition. The coefficient scalar functions G_A and $G_{\partial A}$ of velocity field components V_n and V_t are called the shape gradient density function and are distributed on the surface and on the boundary respectively. The vector functions $G_A\boldsymbol{n}$ and $G_{\partial A}\mathbf{t}$ are called the shape gradient function. Equations (12), (15) and (16) imply that when the Lagrange functional L has the minimum (i.e. $\dot{L}$), both the mean curvature on the surface and the curvature on the boundary vanish (i.e. $H_A=H_{\partial A}=0$). If the arbitrary boundary is closed or the variation in the tangential direction to the surface is constrained, the second term on the right-hand side in (12) is omitted.

3.2 Pneumatic membrane structure problem

Consider a problem for minimizing the area of a pneumatic membrane structure subjected to differential pressure like that shown in Fig. 1a. Defining a specified boundary as the geometric constraint condition and an internal volume Ω (i.e., a space bounded by the membrane) as the equality constraint condition (the constraint value is represented as $\hat{\Omega}$), this problem is expressed as

$$\text{Given} \quad A_0, \tag{17}$$

$$\text{find} \quad \boldsymbol{V}\ (\text{or}\ A_s), \tag{18}$$

$$\text{that minimizes} \quad A\left(=\int_A dA\right), \tag{19}$$

$$\text{subject to} \quad \Omega\left(=\int_\Omega d\Omega\right)\hat{\Omega}. \tag{20}$$

The Lagrange functional $\dot{L}$ for this problem is expressed as

$$L(A,\Omega)=\int_A dA+\Lambda_\Omega\left(\int_\Omega d\Omega-\hat{\Omega}\right). \tag{21}$$

The material derivative $\dot{L}$ of the Lagrange functional $L$with respect to shape variation is expressed as

$$\dot{L}=<G_A\boldsymbol{n},\boldsymbol{V}>_A+\Lambda'_\Omega\left(\int_\Omega d\Omega-\hat{\Omega}\right),\boldsymbol{V}\in C_\theta, \tag{22}$$

$$G_A=H_A+\Lambda_\Omega. \tag{23}$$

When the constraint condition with regard to the internal volume is satisfied, (22) can be written as

$$\dot{L}=<G_A\mathbf{n},\mathbf{V}>_A,\mathbf{V}\in C_\theta. \tag{24}$$

Equations (23) and (24) imply that when the Lagrange functional L has the minimum (i.e. $\dot{L}$), the mean curvatures have a constant value $-\Lambda_\Omega$ across the entire surface.

3.3 Suspension membrane structure problem

Consider the problem for minimizing the area of a suspension membrane structure like that shown in Fig. 1c. Defining specified fixed points on the boundary as the geometric constraint condition and a perimeter length Γ of the boundary as the equality constraint condition (the constraint value is represented as $\hat{\Gamma}$), this problem is expressed as

$$\text{Given} \quad A_0, \tag{25}$$

$$\text{find} \quad \boldsymbol{V}\ (\text{or}\ A_s), \tag{26}$$

$$\text{that minimizes} \quad A\left(=\int_A dA\right), \tag{27}$$

$$\text{subject to} \quad \Gamma\left(=\int_{\partial A} d\Gamma\right)=\hat{\Gamma}. \tag{28}$$

The Lagrange functional L for this problem is represented as

$$L(A,\Gamma)=\int_A dA+\Lambda_\Gamma\left(\int_{\partial \mathrm{A}} d\Gamma-\hat{\Gamma}\right). \tag{29}$$

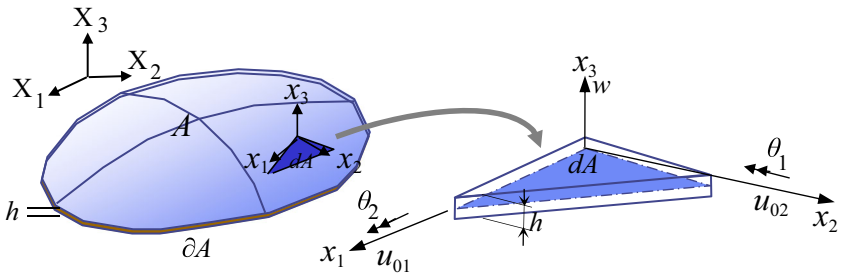

Fig. 3 Coordinates system of pseudo-elastic shell structure consists of a set of infinitesimal flat surfaces

If the constrained perimeter condition is satisfied, the material derivative $\dot{L}$ of the Lagrange functional L with respect to shape variation is represented as

$$\dot{L} =< G_A \boldsymbol{n}, \boldsymbol{V} >_A + < G_{\partial A} \boldsymbol{t}, \boldsymbol{V} >_{\partial A}, \quad \boldsymbol{V} \in C_\theta, \tag{30}$$

$$G_A = H_A, \tag{31}$$

$$G_{\partial A} = 1 + \Lambda_\Gamma H_{\partial A}. \tag{32}$$

The shape gradient functions derived here are used for determining the optimal shape (or the optimal design velocity field or the optimal shape variation). We will explain the method in the next section.

4 Free-form optimization method for form-finding of membranes

4.1 Free-form optimization method

The free-form optimization method was proposed by one of the authors, and solutions to optimal shape design problems of shells (Shimoda and Tsuji 2006; Shimoda and Liu 2014) and frame structures (Shimoda et al. 2014) have been proposed so far. This distributed-parameter shape optimization method is based on the traction method (Azegami 1994) which is a gradient method in the Hilbert space with a PDE smoother, and can treat all nodes as design variables without parameterization. In this study, we apply the free-form optimization method for shells to various membrane structures in order to find the optimal free-form of membrane structures, i.e., minimal surface with respect to the in-plane shape variation (Shimoda and Tsuji 2006) and the out-of-plane variation (Shimoda and Liu 2014) under some constraint conditions.

In order to determine the shape variation, or the design velocity field that minimizes the objective functional using both the derived shape gradient function and this gradient method in the Hilbert space, a tensor with positive definitiveness must be introduced. Unfortunately, a unit tensor only having a diagonal component cannot maintain the smoothness of the shape since it leads to a jagged problem (Braibant and Fleury 1984). For this reason, a stiffness tensor of an elastic shell under the Robin boundary condition similar in shape to a membrane is used in this method to make the computation simple and linear. It is assumed for simplicity that a shell structure consists of a set of infinitesimal flat surfaces. The stiffness tensor serves not only to reduce the objective functional, but also to maintain the mesh smoothness. The Robin condition with spring constant α is employed to stabilize the convergence (Shimoda and Liu 2014). With this method, the optimal design velocity field $\boldsymbol{V}$ is obtained as the displacement fields by applying the fictitious distributed traction force in proportion to the negative shape gradient function to this pseudo-elastic shell. The current shape is updated by adding the optimal design

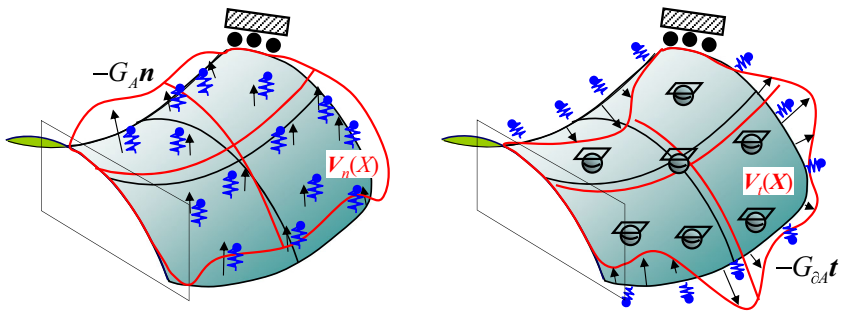

Fig. 4 Schematics of the velocity analyses for membranes

(a) Out-of-plane shape variation (b) In-plane shape variation

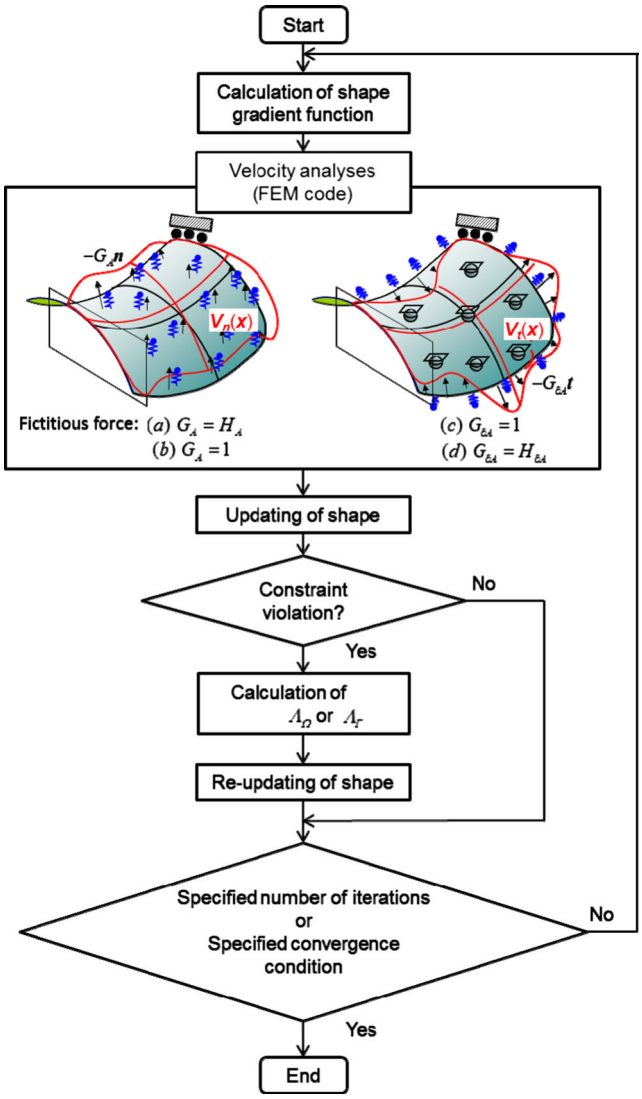

Fig. 5 Flowchart for the free-form optimization method

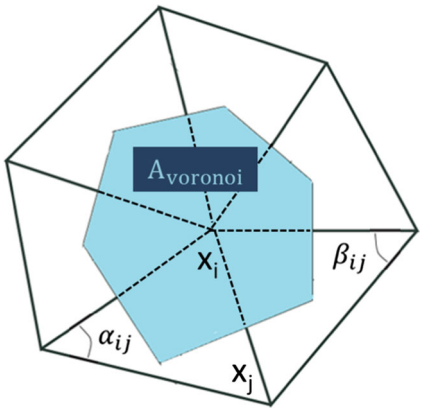

Fig. 6 Definition of Voronoi region area

velocity field $\boldsymbol{V}$. The design velocity field $\boldsymbol{V} = \{V_i\}_{i=1,2,3}$ can be divided into the in-plane component $\boldsymbol{V}_0 = \{V_{0\beta}\}_{\beta=1,2}$ and the out-of-plane component V_3 on the local Cartesian coordinates (x_1, x_2, x_3). Using Kirchhoff's theorem as a plate bending theory, the weak formed governing equations for the out-of-plane shape variation and the in-plane shape variation design velocity field are expressed as (33) and (35), respectively.

$$a((\boldsymbol{V}_0, V_3), \overline{\boldsymbol{U}}) + \alpha \left\langle (\boldsymbol{V}\cdot\boldsymbol{n})\boldsymbol{n}, \overline{\boldsymbol{U}} \right\rangle_A = - < G_A\boldsymbol{n}, \overline{\boldsymbol{U}} >_A, \quad (\boldsymbol{V}_0, V_3) \in C_\Theta, \ \forall \overline{\boldsymbol{U}} \in C_\Theta, \tag{33}$$

$$C_\Theta = \{(\boldsymbol{V}_0, V_3) \in (H^2(A))^3 \mid$$

$$(\boldsymbol{V}_0, V_3 \textit{ satisfy the constraints of shape variation on } A\}. \tag{34}$$

$$a((\boldsymbol{V}_0, V_3), \overline{\boldsymbol{U}}) \ + \alpha \left\langle (\boldsymbol{V}\cdot\boldsymbol{t})\boldsymbol{t}, \overline{\boldsymbol{U}} \right\rangle_{\partial A} = - < G_{\partial A}\boldsymbol{t}, \overline{\boldsymbol{U}} >_{\partial A}, \quad (\boldsymbol{V}_0, V_3) \in C_\Theta, \ \forall \overline{\boldsymbol{U}} \in C_\Theta, \tag{35}$$

$$C_\Theta = \{(\boldsymbol{V}_0, V_3) \in (H^1(A))^3 \Big| \quad (\boldsymbol{V}_0, V_3) \textit{ satisfy the constraints of shape variation on } S \textit{ and } V_3 = 0 \textit{ on } A\}. \tag{36}$$

Here, the bilinear form $a(\cdot\ ,\ \cdot)$, which denotes virtual work related to internal force, and the linear forms $< \cdot\ , \cdot >_A$, $< \cdot\ , \cdot >_{\partial A}$ are expressed as (37), (38) and (39), respectively.

$$a((\boldsymbol{u}_0, w), \overline{\boldsymbol{U}}) = \int_A \{c^B_{\alpha\beta\gamma\delta}\kappa_{\gamma\delta}\bar{\kappa}_{\alpha\beta} + c^M_{\alpha\beta\gamma\delta}\varepsilon_{0\gamma,\delta}\bar{\varepsilon}_{0\alpha,\beta}\} dA, \tag{37}$$

$$< G_A\boldsymbol{n}, \overline{\boldsymbol{U}} >_A = \int_A G_A\boldsymbol{n}\overline{\boldsymbol{U}} dA, \tag{38}$$

$$< G_{\partial A}\boldsymbol{t}, \overline{\boldsymbol{U}} >_{\partial A} = \int_{\partial A} G_{\partial A}\boldsymbol{t}\overline{\boldsymbol{U}} d\Gamma, \tag{39}$$

where $c^B_{\alpha\beta\gamma\delta}$, $c^M_{\alpha\beta\gamma\delta}$ denote the stiffness tensors with respect to bending and membrane stresses, respectively, and can be arbitrarily selected considering the magnitude of shape variation. $\{\kappa_{\alpha\beta}\}_{\alpha,\beta=1,2}$ and $\{\varepsilon_{0\alpha\beta}\}_{\alpha,\beta=1,2}$ denote the curvature

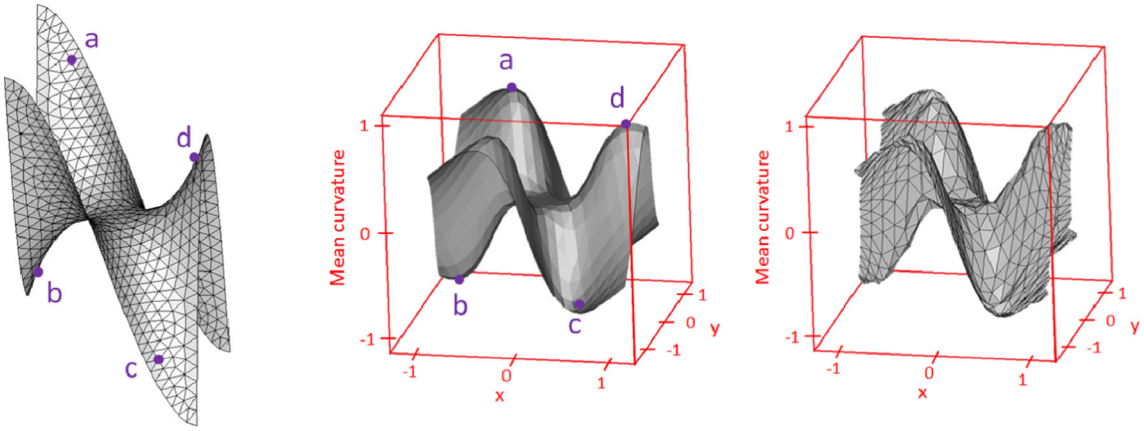

(a) Discretized monkey saddle (b) Theoretical mean curvatures (c) Approximate mean curvatures calculated by Eq. (51)

Fig. 7 Monkey saddle and mean curvatures

tensor and the strain tensor at the mid-plane, respectively, which are defined as

$$\kappa_{\alpha\beta} \equiv \frac{1}{2}(w_{,\alpha\beta} + w_{,\beta\alpha}), \tag{40}$$

$$\varepsilon_{0\alpha\beta} \equiv \frac{1}{2}(u_{0\alpha,\beta} + u_{0\beta,\alpha}). \tag{41}$$

In (33) and (35), the notation $\bar{(\cdot)}$ expresses a variation and $\overline{\boldsymbol{U}}$ is defined as $\overline{\boldsymbol{U}} = (\overline{\boldsymbol{U}}_0, \bar{w})^T$. w and $\boldsymbol{u}_0 = \{u_{0\alpha}\}_{\alpha=1,2}$ represent the out-of-plane displacement and the in-plane displacement vector at the mid-plane on the local Cartesian coordinates (x_1, x_2, x_3), respectively, as shown in (42), (43) and Fig. 3. $\{\theta_\alpha\}_{\alpha=1,2}$ is defined as $\theta_\alpha(x_1, x_2) \equiv \frac{\partial w(x_1,x_2)}{\partial x_\alpha}$ in Fig. 3.

$$u_\alpha(x_1, x_2, x_3) = u_{0_\alpha}(x_1, x_2) - x_3\theta_\alpha, \tag{42}$$

$$u_3(x_1, x_2, x_3) = w(x_1, x_2), \tag{43}$$

With (33) , the optimal out-of-plane shape variation for reducing the membrane area is determined by applying the fictitious distributed traction force $-G_A$ in the normal direction to the pseudo-elastic shell surface. With (35) , in contrast, the optimal in-plane shape variation for reducing the membrane area is determined by applying the fictitious distributed traction force $-G_{\partial A}$ in the tangential direction to the pseudo-elastic shell surface, or in the normal direction to the shell boundary. In the in-plane shape variation analysis, the out-of-plane velocity is constrained (i.e., $V_3 = 0$). We call these analyses for $\boldsymbol{V}$ "velocity analysis". Figure 4 shows schematics of the velocity analyses for (a) out-of-plane shape variation and (b) in-plane shape variation. After each design velocity field is determined separately, they can be combined by using the relation $\boldsymbol{V} = V_n\boldsymbol{n} + V_t\boldsymbol{t}$ according to the membrane type. The magnitude of the fictitious distributed traction force gradually becomes small in the shape changing process, since the mean curvature in the shape gradient function approaches zero or a constant according to the membrane type. We can say this is a natural step-length correction.

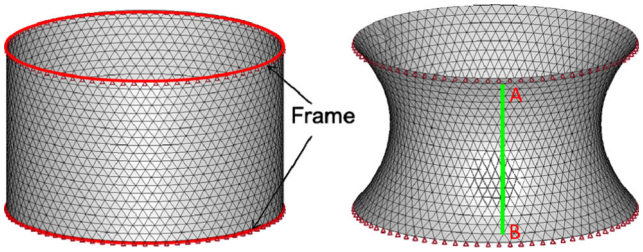

(a) Initial shape (b) Optimal shape

Fig. 8 Optimization result of frame membrane structure (catenoid)

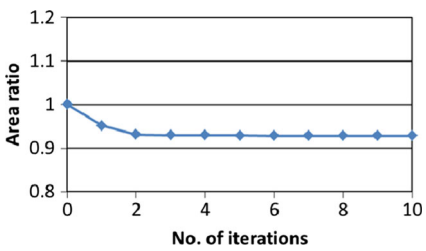

Fig. 9 Iteration histories

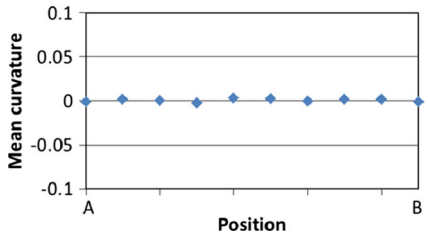

Fig. 10 Mean curvatures along A-B

The fact that the design velocity field $\boldsymbol{V}$ obtained by the velocity analysis, i.e. (33) and/or (35) decreases the objective functional is verified as noted below. In the case of (33), when the constraint condition equation is met, the perturbation expansion of the Lagrange functional L is written as

$$\Delta L = \langle G_A \boldsymbol{n}, \Delta s \boldsymbol{V} \rangle_A + O(|\Delta s|^2). \tag{44}$$

Substituting (33) into (44) and taking account of the positive definitiveness of $a((\boldsymbol{V}_{0\alpha}, V_3), (\overline{\boldsymbol{u}}_0, \overline{w}))$ and $\alpha \langle (\boldsymbol{V} \cdot \boldsymbol{n})\boldsymbol{n}, (\overline{\boldsymbol{u}}_0, \overline{w}) \rangle$, (45) can be obtained if Δs is sufficiently small.

$$\Delta L = -\{a(\boldsymbol{V}, \Delta s \boldsymbol{V}) + \alpha \langle (\boldsymbol{V} \cdot \boldsymbol{n})\boldsymbol{n}, \Delta s \boldsymbol{V} \rangle_A\} < 0. \tag{45}$$

The same approach can be applied to the case of (35). These relations indicate that, for problems having convexity the Lagrange functional L is necessarily reduced by updating the shape according to the velocity field $\boldsymbol{V}$ determined by the velocity analysis.

4.2 A method for satisfying equality constraint

We use the method proposed as a solution to a multiconstraint problem by the traction method (Shimoda et al. 1995) in order to satisfy the constraint condition (e.g. internal volume or perimeter constraint) according to the type of membrane structure. The free-form optimization method is used under the assumption that the Lagrange multipliers Λ_Ω and Λ_Γ derived in (23) and (32) would satisfy the given constraint. The procedure for determining Lagrange multiplier Λ_Ω or Λ_Γ that satisfy the equality constraint is applied to the pneumatic or suspension membrane structure problem. Since they have only one constraint, the internal volume or the perimeter constraint, respectively, the procedures for them are very simple.

For the internal volume constraint problem, the shape gradient function of (23) is used. Here, let us define the internal volume deviation between the current volume Ω and its constraint value $\hat{\Omega}$ as $\Delta\Omega\,(=\ \hat{\Omega} - \Omega)$ $\Delta\Omega$ is expressed by superposing $\Delta\Omega_H$ and $\Lambda_\Omega \Delta\Omega_U$ as shown in (46) under the assumption that each shape variation is small.

$$\Delta\Omega = \Delta\Omega_{H_A} + \Lambda_\Omega \Delta\Omega_U, \tag{46}$$

where $\Delta\Omega_{H_A}$ is the internal volume variation by the first term $H_A(\boldsymbol{X})$ of the right side of (23) which is applied on the whole membrane surface as the fictitious distributed force, and $\Delta\Omega_U$ is the internal volume variation by the uniform fictitious unit force which is also applied on the whole membrane surface.

So as to satisfy (20), (46) can be arranged as

$$\Lambda_\Omega = \frac{(\hat{\Omega} - \Omega) - \Delta\Omega_{H_A}}{\Delta\Omega_U}. \tag{47}$$

For the perimeter constraint problem, the shape gradient functions of (31) and (32) are used. Here, let us define the perimeter deviation between the current perimeter Γ and its constraint value $\hat{\Gamma}$ as $\Delta\Gamma\ (=\ \hat{\Gamma} - \Gamma)$. $\Delta\Gamma$ is expressed by superposing $\Delta\Gamma_U$, $\Lambda_\Gamma \Delta\Gamma_{H_{\partial A}}$ and $\Delta\Gamma_{H_A}$ as shown in (48).

$$\Delta\Gamma = \Delta\Gamma_U + \Lambda_\Gamma \Delta\Gamma_{H_{\partial A}} + \Delta\Gamma_{H_A}, \tag{48}$$

where $\Delta\Gamma_U$ is the perimeter variation by the uniform fictitious unit force, which is also applied on the whole membrane boundary. $\Delta\Gamma_{H_{\partial A}}$ is the perimeter variation by the second term $H_{\partial A}(\boldsymbol{X})$ of the right side of (32), which is applied on the whole membrane boundary as the fictitious distributed force $\Delta\Gamma_{H_A}$ is the perimeter variation by $H_A(\boldsymbol{X})$ of (31), which is applied on the whole membrane surface as the fictitious distributed force.

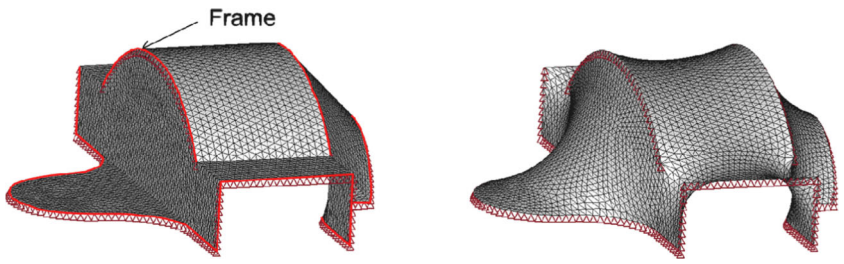

(a) Initial shape (b) Optimal shape

Fig. 11 Optimization result of complicated frame membrane structure

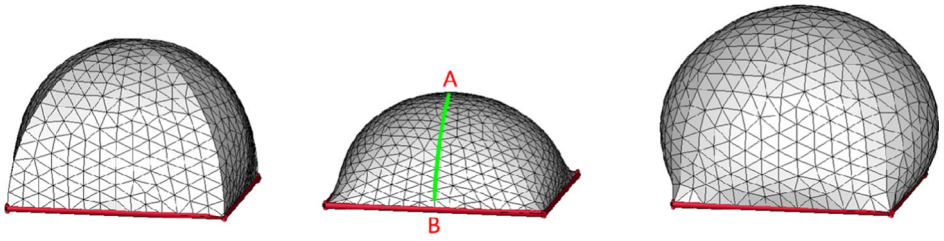

Fig. 12 Optimization results of pneumatic membrane structure

(a) Initial shape (Initial internal volume: V_0) (b) Optimal shape (Constraint volume: V=0.5V_0) (c) Optimal shape (Constraint volume: V=1.5V_0)

So as to satisfy (28), (48) can be arranged as

$$\Lambda_\Gamma = \frac{(\hat{\Gamma} - \Gamma) - \Delta\Gamma_U - \Delta\Gamma_{H_A}}{\Delta\Gamma_{H_{\partial A}}}. \tag{49}$$

The Lagrange multipliers Λ_Ω and Λ_Γ are respectively calculated by (47) and (49), and used in the free-form optimization process, which will be described in the following section.

4.3 Flowchart of free-form optimization

The minimal surface with the optimal free-form can be obtained by repeating the processes shown in Fig. 5. First, the shape gradient function distributed all over the surface is calculated from the information of the current shape. The shape gradient function calculated is not used directly to vary the shape, but replace with the fictitious distributed traction force as stated in Section 4.2. The fictitious traction forces are separately applied to the pseudo elastic shell to satisfy the constraint condition as stated in Section 4.2. In this study, a general-purpose FEM code was used in the velocity analyses. The stiffness tensor of the shell is updated at every iteration loop. One to three fictitious forces out of four ((a) - (d) in Fig. 5) are independently applied to the pseudo-elastic shell in the velocity analyses, depending on the type of membrane structure. For example, fictitious forces (a) $G_A = H_A(\boldsymbol{X})$ and (b) $G_A = 1$ are applied for a pneumatic membrane structure, and the number of FEA runs in each iteration loop is correspondent to the number of fictitious forces. Displacements obtained in the velocity analyses are superposed to the current shape to update the current shape as stated in Section 4.2. If the update shape does not satisfy the constraint condition, then re-updating is done using the Lagrange multiplier which is determined by (47) or (49). The computation is repeated until satisfying the specified number of times or the convergence condition The convergence condition can be set as 0.1 ∼ 0.01 % of the change rate of the objective functional.

4.4 Curvature computation method

The shape gradient functions include twice the mean curvature H_A of the surface and/or the curvature $H_{\partial A}$ of the geometric boundary. Therefore we have to approximately calculate these curvatures at all points of a finite element model to find the minimal surface using our method explained in the previous section. Many methods have been proposed so far for calculating the approximate curvature of a discretized surface, and here we make use of a discrete method proposed by Meyer et al. (2002). Consider the elements around a node x_i as shown in Fig. 6. The Voronoi region area is defined as

$$A_{\text{voronoi}} = \frac{1}{8}\sum \left(\cot\alpha_{ij} + \cot\beta_{ij}\right) \left\| x_i - x_j \right\|^2. \tag{50}$$

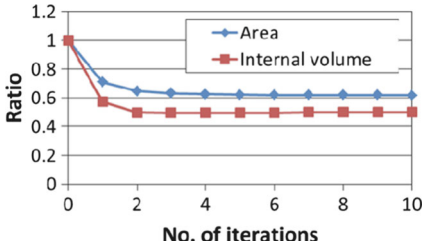

Fig. 13 Iteration histories

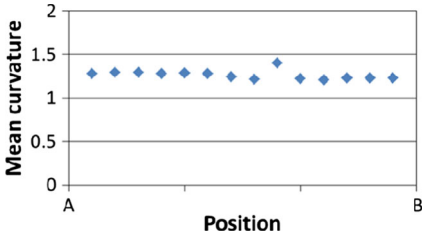

Fig. 14 Mean curvatures along A-B

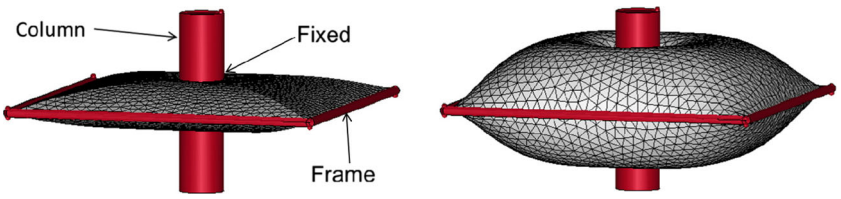

(a) Initial shape (b) Optimal shape

Fig. 15 Optimization result of pneumatic membrane structure with a frame

Using this area, the mean curvature is calculated as

$$\boldsymbol{H}(x_i) = \frac{1}{2A_{\text{voronoi}}} \times \sum \left(\cot \alpha_{ij} + \cot \beta_{ij}\right)\left(x_i - x_j\right). \quad (51)$$

Figure 7c shows the results obtained when (51) was applied to a discretized monkey-saddle function as shown in Figs. 7a and 7b to confirm its validity. It is seen that the calculated values almost correspond to theoretical ones.

5 Numerical results of minimal surface

5.1 Frame membrane structure problem (area minimization)

In order to verify the validity of this form-finding method for frame membrane structures, it was applied to a problem for finding a catenoid known as one of the minimal surfaces. The initial shape of a cylinder, both ends of which were framed as the specified boundaries is shown in Fig. 8a. In the velocity analysis the boundaries were simply supported. The minimal surface shown in Fig. 8b was determined by the out-of-plane variation according to the shape gradient density function (15), i.e. fictitious force (a) in Fig. 5, since all edges were closed. Figures 9 and 10 show the iteration convergence histories of the area and the mean curvatures of the optimal shape along A-B. FEA was run 10 times in total since the sequence of the computation was repeated 10 times as shown in Fig. 9 (i.e. the number of iteration loops was 10). The results show that the shape obtained is a well-approximated catenoid with smoothness. The area decreased by around 7 % and converged steadily while the mean curvatures almost vanished similar to the theoretical value. The change rate of objective functional at the last updating was −0.01 %.

Likewise, an area minimization analysis was performed for a complicated membrane frame structure. The initial shape was framed as shown in Fig. 11a. In the velocity analysis the framed points were simply supported. The minimal surface shown in Fig. 11b was determined by the out-of-plane variation according to the shape gradient density function 15, i.e. fictitious force (a) in Fig. 5. FEA was run 30 times in total since the number of iteration loops was 30. A smooth shape without any mean curvature was obtained. The change rate of objective functional at the last updating was −0.01 %. These results verified the validity of this form-finding method for frame membrane structures.

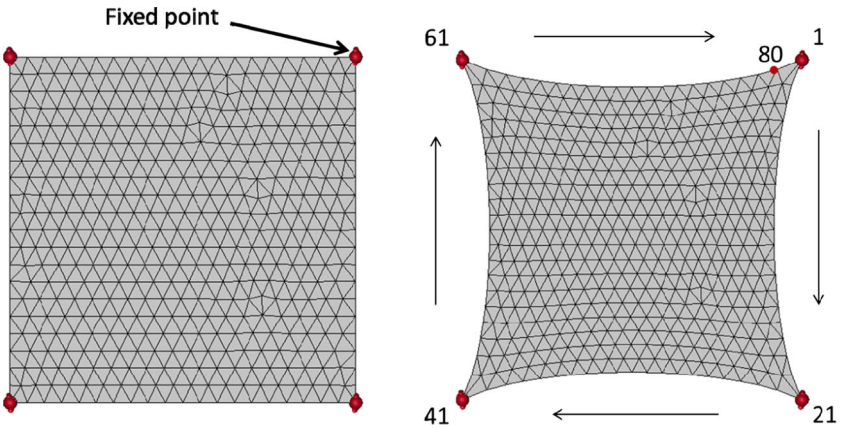

(a) Initial shape (b) Optimal shape

Fig. 16 Optimization result of plane suspension membrane structure

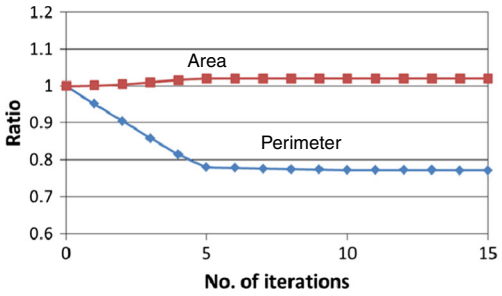

Fig. 17 Iteration histories

5.2 Pneumatic membrane structure problem (area minimization subjected to internal volume constraint)

The initial shape having internal volume, i.e. the space bounded by the membrane, was created as shown in Fig. 12a. Under the two types of internal volume constraint conditions (i.e. 50 % and 150 % of the initial shape), analyses of the minimal surface were respectively conducted using the proposed method. In the velocity analysis, the square boundary was simply supported. The minimal shapes were determined by the out-of-plane variation according to the shape gradient density function (23), i.e. fictitious forces (a) and (b) in Fig. 5. The internal volume was computed by space discretization using tetra elements. Figure 12 shows the optimal shapes subjected to (b) the 50 % constraint and (c) the 150 % constraint of the initial shape. Both have smooth spherical shapes. Figure 13 shows the iteration convergence histories of the area and the internal volume for the 50 % constrained shape. FEA was run 20 times in total since the sequence of the computation was repeated 10 times as shown in Fig. 13. Figure 14 shows the mean curvatures of the final shape along A-B. The graphs show that the area was minimized and reduced by around 48 %, thereby satisfying the internal volume constraint, while the mean curvatures have nearly constant values The change rate of objective functional at the last updating was −0.05 %.

The proposed method was applied to another pneumatic membrane structure with a frame and a column. As the initial shape, the membrane was fixed to the frame and the column as shown in Fig. 15a. The internal volume constraint was set as 300 % of the initial shape. In the velocity analysis, the fixed points were simply supported. The minimal surface was determined by the out-of-plane variation according to the shape gradient density function (23), i.e. fictitious forces (a) and (b) in Fig. 5. Figure 15b shows the optimal shape obtained FEA was run 20 times in total since the number of iteration loops was 10. A smooth shape with a constant mean curvature was created. The change rate of objective functional at the last updating was −0.03 %. This verified that valid results can be obtained for pneumatic membrane structures subjected to an internal volume constraint.

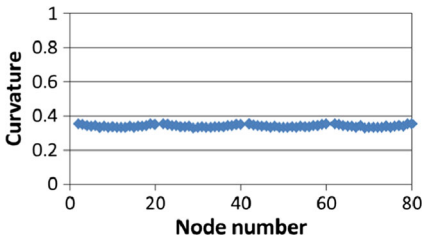

Fig. 18 Curvature distribution on boundary

5.3 Suspension membrane structure problem (area minimization subjected to perimeter constraint)

As the basic problem of suspension membrane structures, an area minimization analysis was conducted under a perimeter constraint condition. The initial shape of a square, the four vertices of which were fixed is shown in Fig. 16a. In the velocity analysis, the vertices were simply supported. The perimeter constraint was set as 102 % of the initial shape. The minimal surface shown in Fig. 16b was determined by the in-plane variation according to the shape gradient density functions (32), i.e. fictitious forces (c) and (d) in Fig. 5. Figure 17 shows the iteration convergence histories of the area and the perimeter. FEA was run 30 times in total since the sequence of the computation was repeated 15 times as shown in Fig. 17. Figure 18 shows the mean curvatures at the nodes numbered from 1 to 80 along the boundary. The graphs show that the area was minimized and reduced by around 23 %, while the perimeter constraint was satisfied. The final shape has a smooth boundary with nearly constant curvatures The change rate of objective functional at the last updating was −0.01 %.

The method was applied to a membrane structure like a tarpaulin, as a practical problem. The initial shape, the six vertices of which were fixed, is shown in Fig. 19a. The perimeter constraint was set as 102 % of the initial shape. In the velocity analysis, the six points were simply supported. The minimal surface was determined by the out-of-plane and in-plane variations according to the shape gradient density functions (31)(32), i.e. fictitious forces (a), (c) and (d) in Fig. 5. Figure 19b shows the optimal shape obtained. FEA was run 150 times in total since the number of iteration loops was 50. The area was minimized and reduced by around 29 %, while the perimeter constraint was satisfied. A smooth surface was obtained with boundary shapes having almost constant curvatures. The change rate of objective functional at the last updating was −0.03 %.

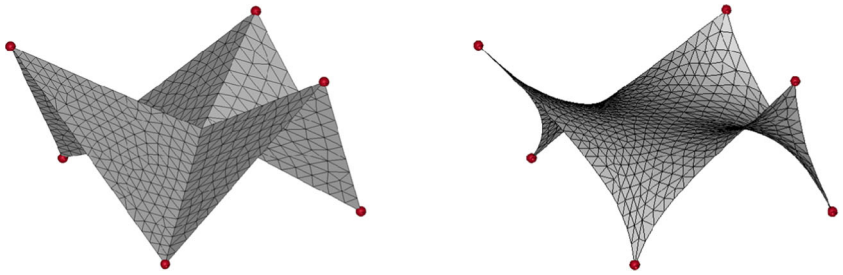

(a) Initial shape (b) Optimal shape

Fig. 19 Optimization result of 6-points spatial suspension membrane structure

Finally, the proposed method was applied to an umbrella-like suspension membrane shown in Fig. 20a. The perimeter constraint value and the boundary condition of the velocity analysis were same as the tarpaulin problem shown in Fig. 19. FEA was run 120 times in total since the number of iteration loops was 40. Figure 20b shows the optimal shape obtained. The area was minimized and reduced by around 11 %, while satisfying the perimeter constraint. The change rate of objective functional at the last updating was −0.01 %.

Although the constraint value of perimeter length or internal volume is applied to a tentative initial shape for designing the final, or the minimal shape of membrane structures in Sections 5.1 to 5.3, the constraint value can be applied to a minimal surface which has already determined by the proposing method. Consider an internal volume constraint is additionally applied to a minimal surface which has already determined, for shrinking or expanding the minimal surface, then the pressure generating pre-stress of the membrane is uniquely calculated by the difference of the volume although the elastic deformation of the membrane is not considered. In contrast, when a perimeter constraint is applied to a minimal surface for shrinking or expanding the minimal surface, the edge force generating pre-stress of the membrane can be uniquely determined by the difference of the area, neglecting the elastic deformation of the membrane. Therefore, when a pre-stress is given in advance, the constraint value for generating the pre-stress by the pressure or the edge force is calculated, and the value is applied to the proposing method in order to determine the new minimal surface for generating the pre-stress.

6 Conclusions

In this paper, we have newly proposed a numerical form-finding method, a non-parametric gradient method with a smoother, for designing membrane structures. Various form-finding problems of membranes were formulated as distributed-parameter shape optimization problems for obtaining an equally tensioned surface (i.e. minimal surface), which is essential for membrane design. A previously-reported free-form optimization method for shells was applied to the membrane structures According to the type of membrane structure (e.g. frame membrane, pneumatic membrane and suspension membrane), the in-plane shape variation and/or the out-of-plane shape variation was defined as the variable for form-finding. By applying the derived sensitivity function to the gradient method in the Hilbert space and determining the optimal design velocity field based on the assumption of small variation, we found the minimal surfaces by iterative computations. With this method, the optimal and smooth free-forms of membranes can be obtained without shape parameterization. The validity and the versatility of the proposed method were verified by the results of the examples examined for each type of membrane structure.

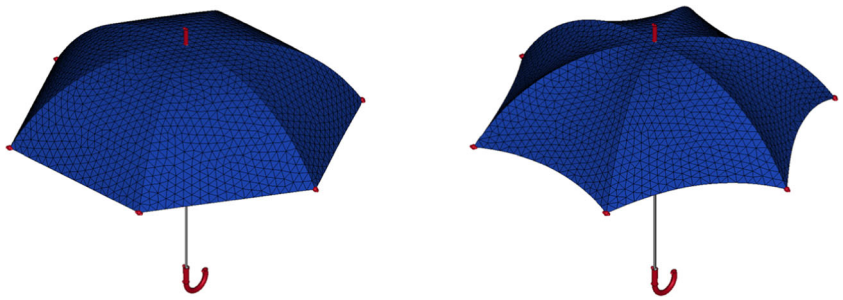

(a) Initial shape (b) Optimal shape

Fig. 20 Optimization result of umbrella-like suspension membrane structure

Acknowledgments A part of this research was supported by grants in-aid from the Research Center of Smart and Tough Machines at the Toyota Technological Institute.

References

Azegami H (1994) A solution to domain optimization problems. Trans Japan Soc Mech Eng 60:1479–1486. (in Japanese)

Bletzinger KU, Wuchner R, Daoud F, Camprubi N (2005) Computational methods for form finding and optimization of shells and membranes. Comput Methods Appl Mech Eng 194(30–33):3438–3452

Bletzinger KU, Firl M, Linhard J, Wuchner R (2010) Optimal shapes of mechanically motivated surfaces. Comput Methods Appl Mech Eng 199(5–8):324–333

Braibant V, Fleury C (1984) Shape optimal design using b-splines. Comput Methods Appl Mech Eng 44(3):247–267

Choi KK, Kim NH (2005) Structural sensitivity analysis and optimization 1. Springer

Gray A (1998) Modern differential geometry of curves and surfaces with MATHEMATICA. CRC Press

Linkwitz K (1999) About formfinding of double-curved structures. Eng Struct 21(8):709–718

Monterde J (2004) Bézier surfaces of minimal area: the Dirichlet approach. Comput Aided Geom Des 21(2):117–136

Meyer M, Desbrun M, Schroder P, Barr AH (2002) Discrete differential-geometry operators for triangulated 2-manifolds. Vis Math III:35–57

Otto F (1973) Tensile structures. MIT Press

Pan Q, Xu G (2011) Construction of minimal subdivision surface with a given boundary. Comput-Aided Des 43:374–380

Shimoda M, Azegami H, Sakurai T (1998) Traction Method approach to optimal shape design problems, SAE 1997 transactions. Journal of Passenger Cars, Section 6(106):2355–2365

Shimoda M, Tsuji J (2006) Non-parametric shape optimization method for rigidity design of automotive sheet metal structure, SAE 2006 Transactions. Journal of Passenger Cars - Mechanical Systems, Paper No. 2006-01-0584, pp 483-492

Shimoda M, Liu Y (2014) A Non-parametric free-form optimization method for shell structures. Struct Multidiscip Optim. doi:10.1007/s00158-014-1059-1

Shimoda M, Liu Y, Morimoto T (2014) Non-parametric free-form optimization method for frame structures. Struct Multidiscip Optim 50(1):129–146

Shimoda M, Azegami H, Sakurai T (1995) shape optimization of linear elastic structures subject to multiple loading conditions. Current Topics in Computational Mechanics 305:319–326